

SurroundDepth: Entangling Surrounding Views for Self-Supervised Multi-Camera Depth Estimation

Yi Wei^{1,2*}, Linqing Zhao^{3*}, Wenzhao Zheng^{1,2}, Zheng Zhu⁴, Yongming Rao^{1,2},

Guan Huang⁴, Jiwen Lu^{1,2,†}, Jie Zhou^{1,2}

¹Beijing National Research Center for Information Science and Technology, China

²Department of Automation, Tsinghua University, China

³School of Electrical and Information Engineering, Tianjin University, China

⁴PhiGent Robotics

Abstract: Depth estimation from images serves as the fundamental step of 3D perception for autonomous driving and is an economical alternative to expensive depth sensors like LiDAR. The temporal photometric constraints enables self-supervised depth estimation without labels, further facilitating its application. However, most existing methods predict the depth solely based on each monocular image and ignore the correlations among multiple surrounding cameras, which are typically available for modern self-driving vehicles. In this paper, we propose a SurroundDepth method to incorporate the information from multiple surrounding views to predict depth maps across cameras. Specifically, we employ a joint network to process all the surrounding views and propose a cross-view transformer to effectively fuse the information from multiple views. We apply cross-view self-attention to efficiently enable the global interactions between multi-camera feature maps. Different from self-supervised monocular depth estimation, we are able to predict real-world scales given multi-camera extrinsic matrices. To achieve this goal, we adopt the two-frame structure-from-motion to extract scale-aware pseudo depths to pretrain the models. Further, instead of predicting the ego-motion of each individual camera, we estimate a universal ego-motion of the vehicle and transfer it to each view to achieve multi-view ego-motion consistency. In experiments, our method achieves the state-of-the-art performance on the challenging multi-camera depth estimation datasets DDAD and nuScenes. Code is available at <https://github.com/weiyithu/SurroundDepth>.

Keywords: Self-supervised depth estimation, Multi-camera perception, Structure-from-motion

1 Introduction

Recent years have witnessed the rapid development of autonomous driving. Instead of relying on expensive depth sensors like LiDAR to perform extract structural information, 3D perception from cameras has become a promising approach and potential alternative due to its semantic richness and economy. Acting as a bridge between the input 2D image and the real 3D environment, depth estimation has a crucial influence on the downstream 3D understanding and receives increasing attention [1, 2, 3, 4, 5, 6, 7, 8, 9, 10].

Due to the expensive cost of densely annotated depth maps, depth estimation is usually learned in a self-supervised manner. By simultaneously predicting the depth maps and the ego-motions of cameras, existing methods take advantage of the temporal photometric constraints between successive images as the supervision signal [11, 12, 13, 14, 15, 16]. Despite that modern self-driving cars

*Equal contribution.

†Corresponding author.

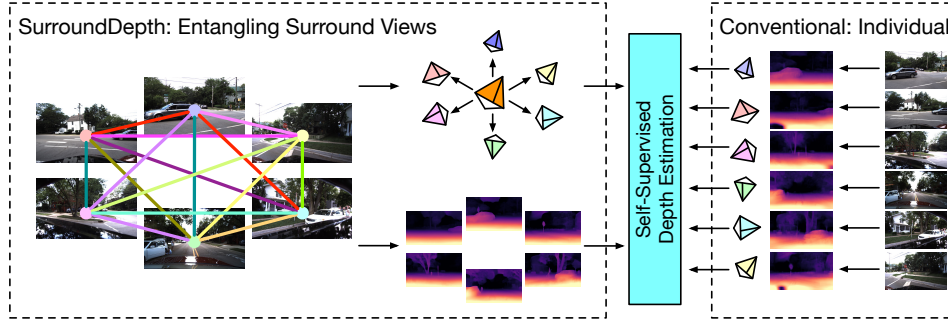


Figure 1: Comparison between SurroundDepth and self-supervised monocular depth estimation methods. Conventional methods [27, 28] predict depths and ego-motions of each view separately, which ignores the correlations between views. Our method incorporates the information across cameras and jointly process all surrounding views.

are usually equipped with multiple cameras to capture the full 360° view of the surrounding scene, most existing methods still focus on predicting depth maps from monocular images and ignore the correlations [17, 18, 19, 20, 21, 22, 23, 24, 25, 26] among the surrounding views [27, 28, 29, 30, 31].

In this paper, we propose SurroundDepth to process all the surrounding views jointly to produce high-quality depth maps across cameras. We first employ a shared encoder to extract high-level feature maps for each view and then propose a cross-view transformer to effectively fuse them. To efficiently allow multi-scale interactions between the features across cameras, we first reduce the resolution of feature maps with depthwise separable convolutions. Then we apply cross-view attention to integrate multi-camera features and use deconvolution to recover the original resolution. To alleviate the information loss induced by feature map downsampling, we add skip connections between individual and interacted feature maps. Finally, we use a shared decoder to attain the predicted depth maps. To recover the real-world scales, we propose Structure-from-Motion (SfM) pretraining and joint pose estimation to predict scale-aware results. In detail, we pretrain the depth estimation model with scale-aware pseudo depths derived from SfM [32]. Joint pose estimation is designed to achieve consistent pose predictions between cameras. By explicitly leveraging extrinsic matrices, we are able to calculate the individual ego-motion of each view from the predicted universal ego-motion. We conduct extensive experiments on the challenging multi-camera depth estimation datasets DDAD [27] and nuScenes [33]. Experimental results show that the cross-view feature interaction boost the performance and the proposed techniques can achieve real-scale depth estimation.

2 Related Work

Self-supervised Monocular Depth Estimation: Without available ground-truths, many approaches explore the routes of learning depths and motions simultaneously [11, 28, 12, 13, 14, 34, 15, 16, 35]. For monocular sequences, the geometric constraints are usually built on adjacent frames. Zhou *et al.* [11] built the problem as a task of view synthesis and trained two networks to separately predict poses and depths. Monodepth2 [28] further enhanced the quality of predictions by proposing the minimum re-projection loss, full-resolution multi-scale sampling, and auto-masking loss, which has been adopted in [36, 37]. Recently, FSM [29] extended self-supervised monocular depth estimation to full surrounding views by introducing both spatial and temporal contexts to enrich the supervision signals. Different from these monocular depth estimation methods, Our SurroundDepth captures cross-view interactions in surrounding views, which are important for fully understanding the environment with multiple cameras.

Additional Supervision for Depth Estimation: Recent approaches introduce additional supervision signals to strengthen the accuracy of depth estimation, such as optical flow [14, 38] and object motion [36, 16]. DispNet [39] was the first work to transfer information from synthetic stereo video datasets to the real-world depth estimation. Besides, Zheng *et al.* [40] proposed a two-module domain adaptive network with a generative adversarial loss to transfer knowledge from the synthetic domain. Some methods adopt auxiliary depth sensors to capture accurate depths, such as LiDAR, to assist depth estimation [41, 42]. To predict the depths with real-world scales, our method lever-

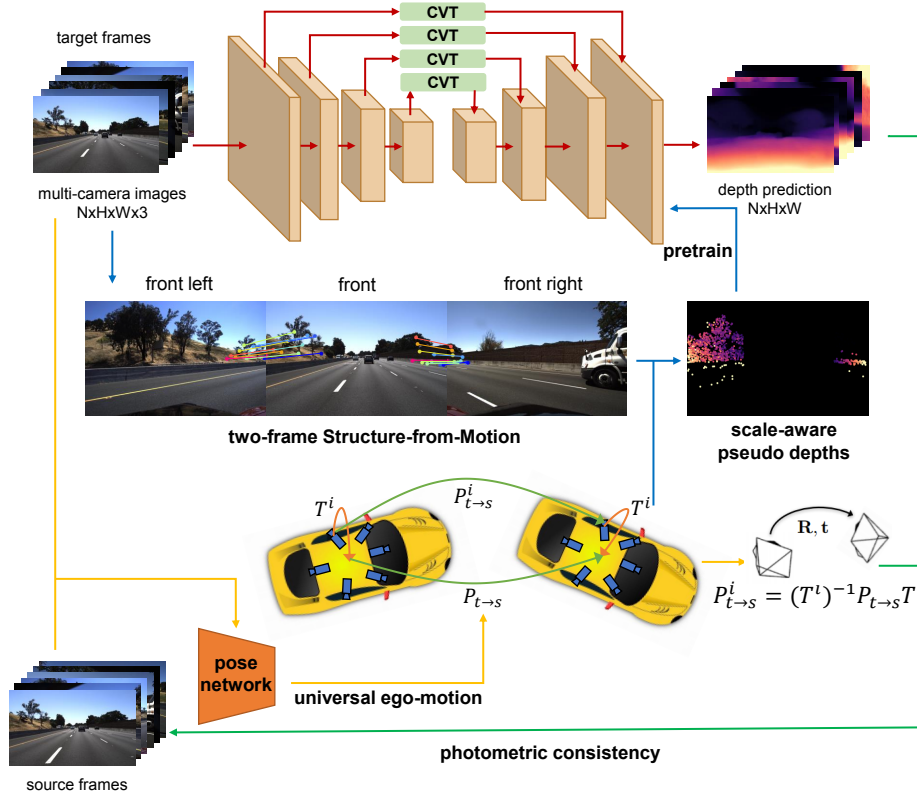


Figure 2: An overview of our SurroundDepth. We utilize encoder-decoder networks to predict depths. To entangle surrounding views, we propose the cross-view transformer (CVT) to fuse multi-camera features in a multi-scale fashion. Pretrained with the sparse pseudo depths generated by two-frame Structure-from-Motion, the depth model is able to learn the absolute scale of the real world. By explicitly introducing extrinsic matrices into pose estimation, we can predict multi-view consistent ego-motions and boost the performance of scale-aware depth estimation.

ages multi-camera extrinsic matrices and takes the sparse depths obtained from SfM to pretrain our network.

3 Approach

3.1 Problem Formulation

In the self-supervised depth and ego-motion settings, the depth network F and pose network G are optimized by minimizing a per-pixel photometric reprojection loss [43, 11]. This reconstruction-based self-supervision paradigm achieves great progress in monocular depth estimation methods [11, 12], and can be directly extended into multi-camera full surround depth estimation. The predicted depth maps and poses of a set of input surrounding samples $I = \{I^1, I^2, \dots, I^N\}$ can be written as:

$$\begin{aligned} D_t &= \{D_t^i\}_{i=1}^N = \{F(I_t^i)\}_{i=1}^N \\ P_{t \rightarrow s} &= \{P_{t \rightarrow s}^i\}_{i=1}^N = \{G(I_t^i, I_s^i)\}_{i=1}^N \end{aligned} \quad (1)$$

where subscript s and t mean the source and target frames. However, estimating full surrounding depths differs from monocular depth estimation in that there exists crucial correlations among the surrounding views, as shown in Figure 1. The overlaps between adjacent views connect all views into a full 360° view of the surroundings, which contains lots of beneficial knowledge and priors for

understanding the whole scene. Based on this fact, we build the joint models to predict depths and ego-motions instead of view-dependent estimations:

$$\begin{aligned} D_t &= \{D_t^i\}_{i=1}^N = F(\{I_t^i\}_{i=1}^N) \\ P_{t \rightarrow s} &= \{P_{t \rightarrow s}^i\}_{i=1}^N = G(\{(I_t^i, I_s^i)\}_{i=1}^N) \end{aligned} \quad (2)$$

Profiting from the joint model, we can not only enable the cross-view information interactions to improve the performance of all views but also generate the universal ego-motion to produce scale-aware predictions with camera extrinsic matrices.

3.2 Overview

As illustrated in Figure 2, the network F can be separated into three parts (*i.e.*, a shared encoder E , a shared decoder D , and several cross-view transformers (CVT)). Given a set of surrounding images, the encoder networks first extract their multi-scale representations in parallel. Different from existing methods that directly decode the learned features, we entangle the features from all views into an integrated feature at each scale, and further utilize multiple scale-specific CVT to perform cross-view self-attentions over all scales. By taking advantage of the powerful attention mechanism, CVT enables each element on the feature maps to propagate its information to other positions and absorb information from others at the same time. Finally, we separate the post-interactive features back to N views and send them to the decoder D .

Unlike monocular depth estimation, we are able to recover the real-world scale from camera extrinsic matrices. A straightforward method to leverage these camera extrinsic matrices is to embed them into spatial photometric loss between two adjacent views. However, we find that the depth network fails to learn the scale directly supervised by spatial photometric loss. To tackle this issue, we propose scale-aware SfM pretraining and joint pose estimation. Specifically, we use two-frame SfM to generate pseudo depths to pretrain the models. The pretrained depth network is able to learn the real-world scale. Moreover, the temporal ego-motions of N cameras have explicit geometric constraints. Instead of using a consistency loss, we estimate the universal pose of the vehicle and calculate the ego-motion of each view according to their extrinsic matrices.

3.3 Cross-View Transformer

With the multi-scale features extracted from all surrounding views, we replace the skip connections between the encoder and decoder with our proposed cross-view transformer (CVT), as shown in Figure 3. Let $X_k \in \mathbb{R}^{N \times H_k \times W_k \times d_k}$ be the feature maps obtained from the k -th scale, and we first supplement each feature with three unique learnable positional encodings (PE_N, PE_H, PE_W), which represent the view-wise, row-wise and column-wise index, respectively.

Then we build Z cross-view self-attention layers to perform the cross-view information exchanging, whose computation cost is $\mathcal{O}(H_k^2 W_k^2 d_k)$ for each layer. However, the cost would be too enormous to accept when processing larger feature maps from the lower layers of the encoder. To avoid the huge cost caused by the quadratic term (*i.e.*, $H_k^2 W_k^2$), we place a depthwise separable convolution (DS-Conv) [44, 45] before attention layers to first summarize the large feature maps into lower-resolution ones with same channel numbers, *i.e.*, $X'_k \in \mathbb{R}^{N \times h_k \times w_k \times d_k}$. With much less computation than a standard convolution, the DS-Conv is widely adopted to balance the trade-off between efficiency and performance. To create the pathway across the features of surrounding views, we flatten the feature maps into an unified sequence, which includes the elements from all views, *i.e.*, $N \times h_k \times w_k$ elements in total. We develop three linear layers to obtain the query, key, and value vectors from $X'_k + PE_N + PE_H + PE_W$, and then we split the features into multiple groups along the channel dimension for multi-head self-attention to enrich the feature diversity. The output features can be represented as:

$$\begin{aligned} O_i^{out} &= \text{Softmax}(K_i^T Q_i / \sqrt{d_k}) V_i \\ X^{out} &= \text{Concat}(O_1^{out}, \dots, O_M^{out}) \end{aligned} \quad (3)$$

where M is the number of feature groups, and K_i, Q_i, V_i denote the i -th feature group of the key, query, and value features, respectively. Benefiting from this attention unit, we ensure that every element on X'_k not only interacts with intra-view features for better understanding of the current frame but also receives inter-view contexts for comprehensive cognition of the scene. To make

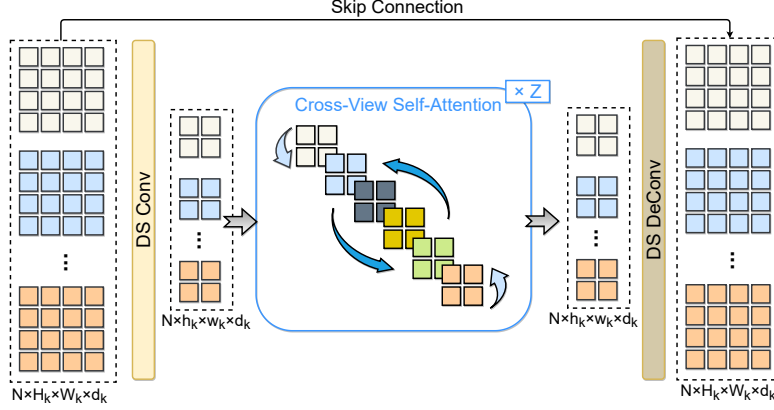


Figure 3: The proposed cross-view transformer. We first use a depthwise separable convolution (DS-Conv) layer to summarize the multi-view features into compact representations. Then we build Z cross-view self-attention layers to fully exchange the flattened multi-view features. After the cross-view interactions, we use a DS-Deconv layer to restore the resolutions of multi-view features. At last, we construct a skip connection to combine the input and restored multi-view features.

cross-view information fully interactive, we stack such unit for Z times in a cascade style. As an inverse process of flattening, we reshape the outputs of the Z -th attention layers back to the shape of $N \times h_k \times w_k \times d_k$, and further upsample the features to the original resolution of input features through a depthwise separable deconvolution. To alleviate the information loss caused by downsampling the feature maps and preserve the input details, we construct a skip connection to directly combine the input and output features:

$$D_k = X_k + X_k^{out} \quad (4)$$

By extending this strategy, features of all scales and all views can be fully propagated and updated from a global perspective.

3.4 Scale-aware Structure-from-Motion Pretraining

The aim of SfM pretraining is to explore the real-world scale from camera extrinsic matrices. A direct way to leverage extrinsic matrices is to use spatial photometric loss between two neighboring views, *i.e.*, warping I_t^i to I_t^j :

$$p_t^{i \rightarrow j} = K^j (T^j)^{-1} T^i D_t^i (K^i)^{-1} p_t^i \quad (5)$$

where K^i, T^i are the intrinsic and extrinsic matrices of i th camera. However, the overlap between I^i and I^j is relatively small, and the $p_t^{i \rightarrow j}$ is easy to be out of the image bounds if the scale of D_t^i is far from the real-world scale. In this way, at the start of the training, the spatial photometric loss will be invalid and cannot supervise the depth network to learn the scale.

To tackle the problem, we first adopt SIFT [46] descriptors to extract correspondences. Then we compute scale-aware pseudo depths by triangulation with camera extrinsic matrices. Finally, we leverage these sparse pseudo depths along with the temporal photometric loss to pretrain the depth and pose networks. However, due to the small overlap and large view changes, the robustness and accuracy of descriptors decrease. To alleviate the issue, we only find corresponding points in a certain region instead of the whole image since we can roughly know the overlapping regions between two neighboring views. Specifically, in this work, we define left $\frac{1}{3}$ part of I^i and right $\frac{1}{3}$ part of I^{i+1} as the valid regions. Further, we leverage epipolar geometry to filter outliers. The epipolar line of point q_m^i can be described as:

$$\begin{aligned} l_m &= F_{i \rightarrow j} q_m^i \\ F_{i \rightarrow j} &= (K^j)^{-T} [t]_{\times} R (K^i)^{-1} \\ [R|t] &= (T^j)^{-1} T^i \end{aligned} \quad (6)$$

where $F_{i \rightarrow j}$ is the fundamental matrix. If the distance between q_m^j and epipolar line l_m is larger than a threshold γ , we regard this correspondence pair as the noise. We provide an example in the supplementary materials.

Method	Abs Rel	Sq Rel	RMSE	RMSE log	$\delta < 1.25$	$\delta < 1.25^2$	$\delta < 1.25^3$
Monodepth2 [28]	0.362	14.404	14.178	0.412	0.683	0.859	0.922
PackNet-SfM [27]	0.301	5.339	14.115	0.395	0.624	0.828	0.908
Monodepth2 -M	0.217	3.641	12.962	0.323	0.699	0.877	0.939
PackNet-SfM -M	0.234	3.802	13.253	0.331	0.672	0.860	0.931
FSM [29]	0.202	-	-	-	-	-	-
FSM* [29]	0.229	4.589	13.520	0.327	0.677	0.867	0.936
SurroundDepth	0.200	3.392	12.270	0.301	0.740	0.894	0.947

Table 1: Comparisons for self-supervised multi-camera depth estimation on DDAD dataset [27]. All methods are trained and tested with the same experimental settings. The results are averaged over all views with median-scaling at test time. -M indicates occlusion masking. * indicates our implementation.

Method	Abs Rel	Sq Rel	RMSE	RMSE log	$\delta < 1.25$	$\delta < 1.25^2$	$\delta < 1.25^3$
Monodepth2 [28]	0.287	3.349	7.184	0.345	0.641	0.845	0.925
PackNet-SfM [27]	0.309	2.891	7.994	0.390	0.547	0.796	0.899
FSM [29]	0.299	-	-	-	-	-	-
FSM* [29]	0.334	2.845	7.786	0.406	0.508	0.761	0.894
SurroundDepth	0.245	3.067	6.835	0.321	0.719	0.878	0.935

Table 2: Comparisons for self-supervised multi-camera depth estimation on the nuScenes dataset [33]. All methods are trained and tested with the same experimental settings. The results are averaged over all views with median-scaling at test time. * indicates our implementation.

3.5 Joint Pose Estimation

An intuitive way of pose estimation is to predict the relative pose of each view separately, which can be represented by Equation 1. However, this strategy ignores the pose consistency between different views, which may lead to ineffective supervision signals. To maintain multi-view ego-motion consistency, we propose to decompose the camera pose estimation problem into two sub-problems: universal pose prediction and universal-to-local transformation. To obtain the universal pose P , we feed N pairs of target and source images into the PoseNet G at a time and take the average of extracted features before the decoder. The universal pose can be computed by:

$$\begin{aligned} \{h^i\}_{i=1}^N &= G_E(\{(I_t^i, I_s^i)\}_{i=1}^N) \\ P_{t \rightarrow s} &= G_D\left(\frac{1}{N} \sum_{i=1}^N h^{(i)}\right) \end{aligned} \quad (7)$$

where G_E and G_D denote the encoder and decoder of PoseNet, respectively. After obtaining the universal pose P , we can further transform it to each camera pose with known camera extrinsic matrices, which can be described as:

$$P_{t \rightarrow s}^i = (T^i)^{-1} P_{t \rightarrow s} T^i \quad (8)$$

where T^i is the extrinsic matrix of i th camera and $P_{t \rightarrow s}^i$ is its ego-motion from target frame to source frame. By combining these two steps, we can obtain the theoretically consistent multi-camera poses, which will further improve the scale-aware depth estimation accuracy.

4 Experiments

4.1 Experimental Setup

We conduct experiments on both the Dense Depth for Automated Driving (DDAD) [27] and nuScenes datasets [33]. The basic backbones of depth and pose networks are the same as the Monodepth2 [28]. We employ ResNet34 with ImageNet [47] pretrained weight as the encoder for all experiments, including baseline methods. Further, surrounding cameras have different focal lengths and we refactor depth maps according to focal lengths following [48]. In each scale, we adopted $Z = 8$ transformer layers and all features were downsampled to 20×12 and 20×11 before cross-view attention on two datasets respectively. Since DDAD dataset has self-occlusion areas, following [29], we annotate occlusion masks manually and use them to reweight photometric loss. More implementation details and visualizations are in supplementary materials.

spatial context	SfM pretrain	joint pose	Abs Rel	Sq Rel	RMSE	RMSE log	$\delta < 1.25$	$\delta < 1.25^2$	$\delta < 1.25^3$
✓			0.967	22.982	31.761	3.518	0.000	0.000	0.000
✓	✓		0.978	24.062	31.980	3.749	0.000	0.000	0.000
✓	✓	✓	0.257	4.565	14.096	0.368	0.557	0.833	0.925
	✓	✓	0.881	19.499	29.552	2.224	0.000	0.001	0.002
✓	✓	✓	0.411	6.121	17.747	0.626	0.089	0.367	0.767
	✓	✓	0.208	3.371	12.977	0.330	0.693	0.871	0.934

Table 3: Quantitative results for scale-aware depth estimation on the DDAD dataset [27]. The scores are averaged over all views **without** median-scaling at test time. ‘spatial context’ denotes whether to use spatial context and multi-camera extrinsic matrices for training.

spatial context	SfM pretrain	joint pose	Abs Rel	Sq Rel	RMSE	RMSE log	$\delta < 1.25$	$\delta < 1.25^2$	$\delta < 1.25^3$
✓			0.978	13.906	18.063	3.967	0.000	0.000	0.000
✓	✓		0.970	13.702	17.931	3.654	0.000	0.000	0.001
✓	✓	✓	0.429	7.839	8.593	0.428	0.471	0.797	0.895
	✓	✓	0.969	13.661	17.896	3.620	0.000	0.000	0.001
	✓	✓	0.363	3.999	8.499	0.479	0.234	0.726	0.876
✓	✓	✓	0.280	4.401	7.467	0.364	0.661	0.844	0.917

Table 4: Quantitative results for scale-aware depth estimation on the nuScenes dataset [33]. The scores are averaged over all views **without** median-scaling at test time. ‘spatial context’ denotes whether to use spatial context and multi-camera extrinsic matrices for training.

4.2 The Benchmark for Multi-camera Depth Estimation

We compare our method with two existing state-of-the-art self-supervised monocular depth estimation methods (Monodepth2 [28] and PackNet-SfM [27]) and one multi-camera depth estimation method FSM [29]. Since FSM does not release code, its detailed experimental setting is unknown, such as evaluation, pretraining and hyperparameters. To fairly compare, we run all methods under the same training and evaluation settings. Specifically, the input images are downsampled to 640×384 and 640×352 resolutions. Depth ground truth is generated by projecting LiDAR point cloud to each view. Since Monodepth2 and PackNet-SfM are not designed for scale-aware depth estimation, we perform per-image median ground truth scaling [11] and post-processing [43] during evaluation. Moreover, SfM pretraining and joint pose estimation are designed for scale-aware depth estimation, we do not adopt them in this experiment. As shown in Tables 1 and 2, our method achieves state-of-the-art performance. Our method outperforms baseline method Monodepth2, which demonstrates that our proposed cross-view approach improves the results since we fully entangle surrounding views. We test inference time of one batch (6 images) on a single RTX 3090: Monodepth2 (0.028s), PackNet-SfM (0.471s), SurroundDepth (0.088s).

4.3 Scale-aware Self-supervised Depth Estimation

Different from monocular depth estimation, once we get the extrinsic matrices of each camera and use spatial context, the absolute scale of the world can be obtained. Tables 3 and 4 show the results without median-scaling at test time. We do not compare other methods since these methods cannot predict scale-aware depth maps. In contrast to the statement in [29], we find that the network directly utilizing spatial photometric loss cannot force the network to generate scale-aware depths. Without pretraining, the scale of initial depth is greatly different from the ground truth, which leads to invalid spatial photometric loss. With our proposed SfM pretraining, the depth network learns the absolute scale and spatial context becomes effective. The joint pose estimation further boosts the performance.

We further evaluate the depth consistency between surrounding views. Specifically, we project each view’s depth map to its neighboring views with extrinsic matrices and calculate depth errors. Table 8 shows that the scale-ambiguous methods such as FSM and Monodepth2 cannot achieve multi-view consistency since the depth maps are scale-ambiguous but extrinsic matrices are scale-aware. With the cross-view interaction, we can further boost the consistency.

skip	multi-scale	Abs Rel	Sq Rel	$\delta < 1.25$
		0.217	3.641	0.699
✓		0.209	3.385	0.704
	✓	0.222	3.763	0.695
✓	✓	0.200	3.392	0.740

Table 5: The ablation study for cross-view transformers. ‘skip’ and ‘multi-scale’ denote skip connection and multi-scale cross-view transformer.

region mask	epipolar filter	Abs Rel	Sq Rel	$\delta < 1.25$
		0.241	3.970	0.629
✓		0.236	3.684	0.649
✓	✓	0.208	3.371	0.693

Table 7: The ablation study for SfM pretraining. ‘region mask’ indicates the region constraint for SIFT matching. ‘epipolar filter’ indicates the epipolar constraints to filter out noisy labels.

4.4 Ablation Study

In this subsection, we conduct ablation studies to verify the effectiveness of each module in our framework. All experiments are conducted on DDAD dataset.

Cross-view Transformer: Table 5 shows that both skip connection and multi-scale formulation contribute to the final results. Skip connections are able to alleviate the information loss caused by the downsampling of feature maps. The multi-scale cross-view transformer helps the network to better learn both fine-grained and global features.

Joint Pose Estimation: Table 6 shows separate pose estimation cannot guarantee the multi-camera pose consistency. To provide a straightforward baseline (second line), we project the ego-motion of all views to the front view and add a loss between the projected and predicted ego-motion of the front view. However, this method gets marginal improvements. We note that our joint pose estimation method gets comparable performances with ground-truth pose experiment. This result indicates that ground truth ego-motion may have noise, even for carefully-calibrated public datasets. Thus, it is necessary to predict accurate scale-aware poses.

Scale-aware SfM Pretraining: Table 7 shows that region mask is able to help our model to learn real-world scale. If we do not set region mask for SIFT matching, we will get wrong correspondences and the depth network is not able to learn real-world scale. By filtering out the correspondences far from the epipolar lines, we will further boost the performance of the depth network.

5 Limitations

Although the proposed SurroundDepth can boost the multi-view depth consistency with scale-aware training strategy and cross-view transformers (as shown in Table 8), our method cannot theoretically guarantee this consistency. As future work, we will directly predict voxel occupancy of the 3D space instead of each view’s depth maps.

6 Conclusion

In this paper, we propose SurroundDepth for self-supervised multi-camera depth estimation. The core insight of our method is to entangle multi-camera information and jointly process all surrounding views. The cross-view transformer is performed at multiple scales to incorporate multi-view features. To obtain scale-aware depth predictions, we present Structure-from-Motion pretraining and joint pose estimation to fully leverage multi-camera extrinsic matrices. Our method achieves state-of-the-art performance on the multi-camera depth estimation datasets.

Pose type	Abs Rel	Sq Rel	$\delta < 1.25$
separate	0.257	4.565	0.557
constraint	0.254	4.390	0.576
joint	0.208	3.371	0.693
ground truth	0.210	4.164	0.729

Table 6: The ablation study for joint pose estimation. ‘separate’ indicates that we predict the pose of each view separately. ‘constraint’ further adds multi-camera consistency constraints.

scale-aware	CVT	Abs Rel	Sq Rel	$\delta < 1.25$
		0.989	28.872	0.000
✓		0.319	18.217	0.732
✓	✓	0.257	8.027	0.735

Table 8: Depth consistency evaluation. ‘scale-aware’ indicates the scale-aware model. ‘CVT’ means cross-view transformers.

Appendix



Figure 4: The occlusion masks of DDAD dataset [27].

A Datasets and Implementation Details

Datasets: We conduct experiments on both the Dense Depth for Automated Driving (DDAD) [27] and nuScenes datasets [33]. The DDAD dataset is a large-scale dataset captured with six synchronized cameras for autonomous driving. The dataset contains 12,650 training samples, including 75,900 images for six cameras. The validation set has 3,950 samples (15,800 images) and ground truth depth maps, which are only utilized for evaluation. During the evaluation procedure, we consider the distance up to 200m and do not crop depth maps. As shown in Figure 4, we can find that each view in DDAD dataset has self-occlusion areas caused by the current vehicle. Following [29], we annotate occlusion masks manually and use them to reweight photometric loss. The nuScenes [33] dataset consists of 1000 sequences of various scenes captured in both Boston and Singapore, where each sequence is approximately 20 seconds long. The dataset is officially partitioned into training, validation, and testing subsets with 700, 150, and 150 sequences, respectively. For each sample, we have access to the six surrounding cameras as well as the camera calibrations. We filter out static frames in nuScenes dataset.

Implementation Details: We use Adam [49] as our optimizer with $\beta_1 = 0.9$ and $\beta_2 = 0.999$. The initial learning rate is set as $1e-4$. For both spatial and temporal photometric loss, we utilize 2 neighboring frames as source frames. Specifically, I_{t-1}^i, I_{t+1}^i and I_t^{i-1}, I_t^{i+1} frames are used as temporal and spatial contexts. Following Monodepth2 [28], we set SSIM weight as 0.85 and depth smoothness weight as $1e-3$.

B Evaluation Metrics

The detailed evaluation metrics of self-supervised depth estimation can be described as follows:

- Abs Rel: $\frac{1}{|T|} \sum_{d \in T} |d - d^*|/d^*$
- Sq Rel: $\frac{1}{|T|} \sum_{d \in T} \|d - d^*\|^2/d^*$
- RMSE: $\sqrt{\frac{1}{|T|} \sum_{d \in T} \|d - d^*\|^2}$
- RMSE log: $\sqrt{\frac{1}{|T|} \sum_{d \in T} \|\log d - \log d^*\|^2}$
- $\delta < t$: % of d s.t. $\max(\frac{d}{d^*}, \frac{d^*}{d}) = \delta < t$

where d and d^* indicate predicted and groundtruth depths respectively, and T indicates all pixels on the depth image D . During evaluation, conventional self-supervised monocular depth estimation methods use the factor $\frac{\text{median}(D^*)}{\text{median}(D)}$ to align the scale. However, in scale-aware experiments, we do not need to perform this scale alignment.

C Scale-aware Structure-from-Motion Pretraining

We provide an example to show the effectiveness of our scale-aware pretraining in Figure 5. As an alternative way to leverage SfM points, we simultaneously use SfM pseudo depths and temporal-spatial photometric loss to supervise the model. From Table 9, we find that since SfM points are sparse and non-uniform and cannot provide strong supervision, this method will get worse results.

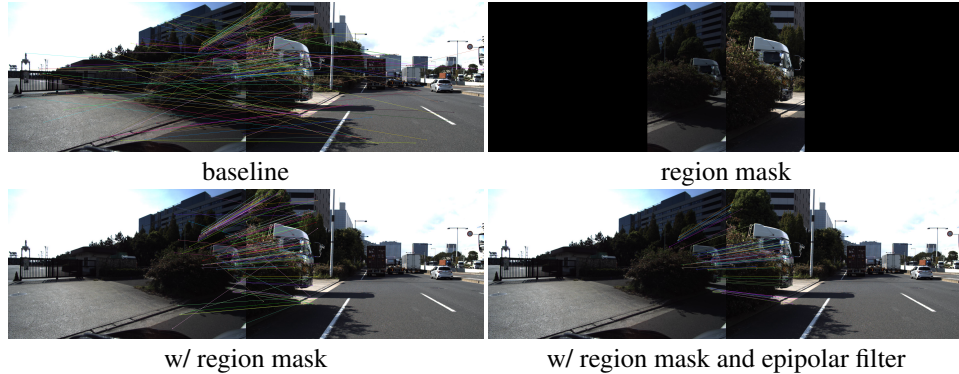


Figure 5: Scale-aware SfM pretraining. Due to the small overlap and large view changes, conventional two-frame Structure-from-Motion will produce many wrong correspondences. By introducing region masks, we reduce the correspondences searching scope and improve the quality. With the camera extrinsic matrices, we can further filter outliers leveraging epipolar geometry. **Better viewed when zoomed in.**

Method	Abs Rel	Sq Rel	$\delta < 1.25$
pretrain	0.286	4.698	0.550
joint train	0.259	4.177	0.619
finetune	0.208	3.371	0.693

Table 9: The ablation study for training method. ‘pretrain’ indicates the performance of SfM pre-trained model. ‘joint train’ means that we simultaneously use SfM pseudo depths and temporal-spatial photometric loss to supervise the networks.

Further, the pretrained model is not good enough and we need to finetune them with spatial and temporal photometric loss.

D Visualization

Qualitative Results Fig. 6 shows qualitative results on DDAD validation set. Our SurroundDepth can predict visually appealing results on all six views. For the occlusion areas, our method can surprisingly inpaint them and predict correct depths. Moreover, the generated depth maps preserve the texture details of corresponding RGB images.

Attention Distribution We visualize cross-view attention maps at the smallest scale in Fig. 7. For a set of query points, the cross-view attention maps can highlight the feature map at the corresponding locations in other views, demonstrating that our cross-attentions are able to entangle multi-view features to predict depths jointly.

Acknowledgments

This work was supported in part by the National Key Research and Development Program of China under Grant 2017YFA0700802, in part by the National Natural Science Foundation of China under Grant 62125603 and Grant U1813218, in part by a grant from the Beijing Academy of Artificial Intelligence (BAAI).

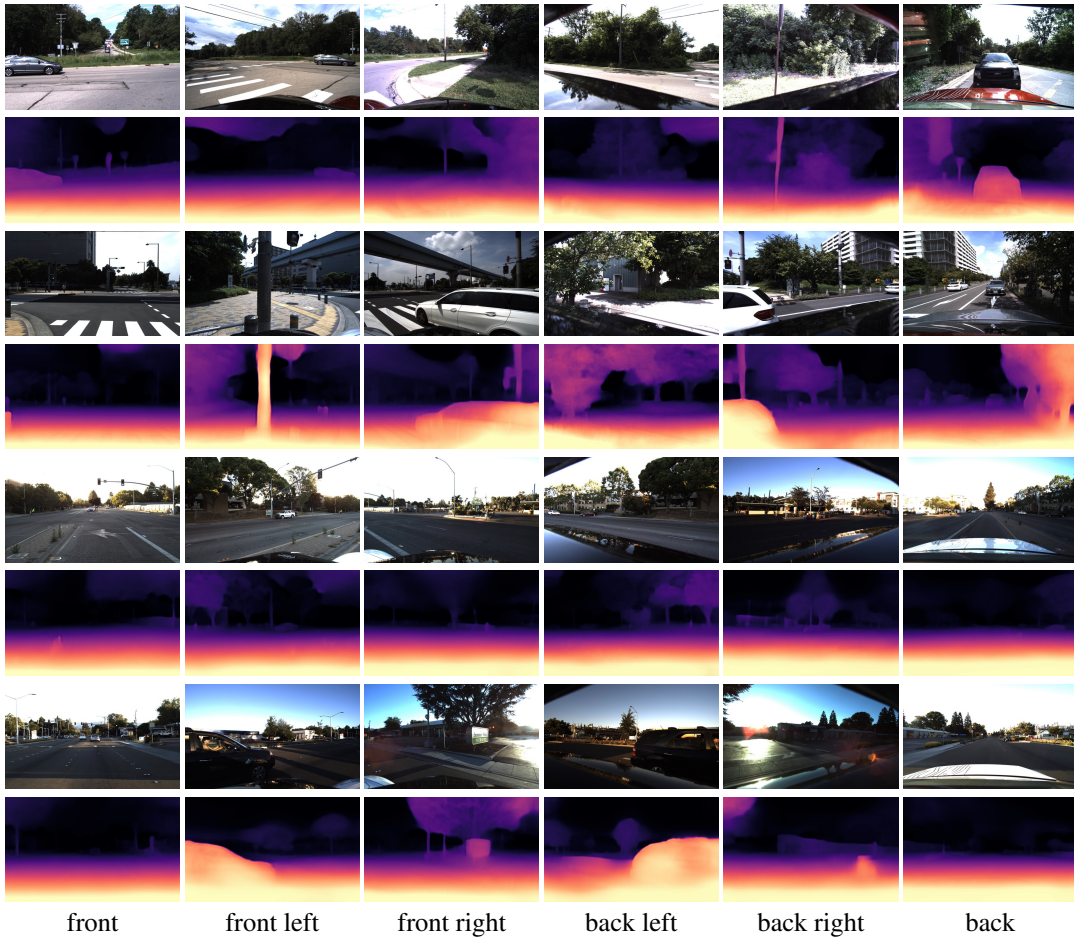


Figure 6: Qualitative results on DDAD [27] dataset. Our method can predict visually appealing depth maps with texture details. **Better viewed when zoomed in.**



Figure 7: The visualization of cross-view attention maps. Given a set of query points, our cross-view attention maps will highlight those features at the corresponding locations in other views. The peaks of attention maps tend to appear in the overlapping areas of adjacent images, which proves that our CVT can accurately entangle the features from multiple views to achieve joint prediction. The predictions are made on the validation set at the smallest scale. **Better viewed when zoomed in.**

References

- [1] B. Li, C. Shen, Y. Dai, A. Van Den Hengel, and M. He. Depth and surface normal estimation from monocular images using regression on deep features and hierarchical crfs. In *CVPR*, pages 1119–1127, 2015.
- [2] P. Wang, X. Shen, Z. Lin, S. Cohen, B. Price, and A. L. Yuille. Towards unified depth and semantic prediction from a single image. In *CVPR*, pages 2800–2809, 2015.
- [3] A. Roy and S. Todorovic. Monocular depth estimation using neural regression forest. In *CVPR*, pages 5506–5514, 2016.
- [4] F. Liu, C. Shen, G. Lin, and I. Reid. Learning depth from single monocular images using deep convolutional neural fields. *TPAMI*, 38(10):2024–2039, 2015.
- [5] H. Fu, M. Gong, C. Wang, K. Batmanghelich, and D. Tao. Deep ordinal regression network for monocular depth estimation. In *CVPR*, pages 2002–2011, 2018.
- [6] M. Song, S. Lim, and W. Kim. Monocular depth estimation using laplacian pyramid-based depth residuals. *TCSVT*, 2021.
- [7] Y. Cao, T. Zhao, K. Xian, C. Shen, Z. Cao, and S. Xu. Monocular depth estimation with augmented ordinal depth relationships. *TCSVT*, 2020.
- [8] J. Huang, G. Huang, Z. Zhu, Y. Yun, and D. Du. Bevdet: High-performance multi-camera 3d object detection in bird-eye-view. *arXiv preprint arXiv:2112.11790*, 2021.
- [9] Z. Li, W. Wang, H. Li, E. Xie, C. Sima, T. Lu, Y. Qiao, and J. Dai. Bevformer: Learning bird’s-eye-view representation from multi-camera images via spatiotemporal transformers. *arXiv preprint arXiv:2203.17270*, 2022.
- [10] Y. Wang, V. C. Guizilini, T. Zhang, Y. Wang, H. Zhao, and J. Solomon. Detr3d: 3d object detection from multi-view images via 3d-to-2d queries. In *CoRL*, pages 180–191, 2022.
- [11] T. Zhou, M. Brown, N. Snavely, and D. G. Lowe. Unsupervised learning of depth and ego-motion from video. In *CVPR*, pages 1851–1858, 2017.
- [12] J.-W. Bian, Z. Li, N. Wang, H. Zhan, C. Shen, M.-M. Cheng, and I. Reid. Unsupervised Scale-consistent Depth and Ego-motion Learning from Monocular Video. In *NeurIPS*, pages 35–45, 2019.
- [13] W. Zhao, S. Liu, Y. Shu, and Y.-J. Liu. Towards Better Generalization: Joint Depth-Pose Learning without PoseNet. In *CVPR*, 2020.
- [14] Z. Yin and J. Shi. Geonet: Unsupervised learning of dense depth, optical flow and camera pose. In *CVPR*, pages 1983–1992, 2018.
- [15] J. Zhou, Y. Wang, K. Qin, and W. Zeng. Moving Indoor: Unsupervised Video Depth Learning in Challenging Environments. In *ICCV*, pages 8618–8627, 2019.
- [16] A. Ranjan, V. Jampani, L. Balles, K. Kim, D. Sun, J. Wulff, and M. J. Black. Competitive Collaboration: Joint Unsupervised Learning of Depth, Camera Motion, Optical Flow and Motion Segmentation. In *CVPR*, pages 12240–12249, 2019.
- [17] X. Chen, H. Ma, J. Wan, B. Li, and T. Xia. Multi-view 3d object detection network for autonomous driving. In *CVPR*, pages 1907–1915, 2017.
- [18] C. Mitash, K. E. Bekris, and A. Boularias. A self-supervised learning system for object detection using physics simulation and multi-view pose estimation. In *IROS*, pages 545–551, 2017.
- [19] A. Laddha, S. Gautam, S. Palombo, S. Pandey, and C. Vallespi-Gonzalez. Mvfusenet: Improving end-to-end object detection and motion forecasting through multi-view fusion of lidar data. In *CVPR*, pages 2865–2874, 2021.

- [20] P.-H. Huang, K. Matzen, J. Kopf, N. Ahuja, and J.-B. Huang. Deepmvs: Learning multi-view stereopsis. In *CVPR*, pages 2821–2830, 2018.
- [21] Y. Yao, Z. Luo, S. Li, T. Fang, and L. Quan. Mvsnet: Depth inference for unstructured multi-view stereo. In *ECCV*, pages 767–783, 2018.
- [22] Y. Wei, S. Liu, Y. Rao, W. Zhao, J. Lu, and J. Zhou. Nerfingmvs: Guided optimization of neural radiance fields for indoor multi-view stereo. In *ICCV*, pages 5610–5619, 2021.
- [23] J. Yang, W. Mao, J. M. Alvarez, and M. Liu. Cost volume pyramid based depth inference for multi-view stereo. In *CVPR*, pages 4877–4886, 2020.
- [24] A. Kundu, X. Yin, A. Fathi, D. Ross, B. Brewington, T. Funkhouser, and C. Pantofaru. Virtual multi-view fusion for 3d semantic segmentation. In *ECCV*, pages 518–535. Springer, 2020.
- [25] A. Dai and M. Nießner. 3dmv: Joint 3d-multi-view prediction for 3d semantic scene segmentation. In *ECCV*, pages 452–468, 2018.
- [26] A. Ouaknine, A. Newson, P. Pérez, F. Tupin, and J. Rebut. Multi-view radar semantic segmentation. In *CVPR*, pages 15671–15680, 2021.
- [27] V. Guizilini, R. Ambrus, S. Pillai, A. Raventos, and A. Gaidon. 3d packing for self-supervised monocular depth estimation. In *CVPR*, pages 2485–2494, 2020.
- [28] C. Godard, O. Mac Aodha, M. Firman, and G. J. Brostow. Digging into self-supervised monocular depth estimation. In *ICCV*, pages 3828–3838, 2019.
- [29] V. Guizilini, I. Vasiljevic, R. Ambrus, G. Shakhnarovich, and A. Gaidon. Full surround monodepth from multiple cameras. *arXiv preprint arXiv:2104.00152*, 2021.
- [30] C. Wang, J. Miguel Buenaposada, R. Zhu, and S. Lucey. Learning depth from monocular videos using direct methods. In *CVPR*, pages 2022–2030, 2018.
- [31] T. Shen, L. Zhou, Z. Luo, Y. Yao, S. Li, J. Zhang, T. Fang, and L. Quan. Self-Supervised Learning of Depth and Motion Under Photometric Inconsistency. In *ICCVW*, pages 0–0, 2019.
- [32] J. L. Schonberger and J.-M. Frahm. Structure-from-motion revisited. In *CVPR*, pages 4104–4113, 2016.
- [33] H. Caesar, V. Bankiti, A. H. Lang, S. Vora, V. E. Liong, Q. Xu, A. Krishnan, Y. Pan, G. Baldan, and O. Beijbom. nuscenes: A multimodal dataset for autonomous driving. In *CVPR*, pages 11621–11631, 2020.
- [34] Z. Wang, L. Tang, X. Liu, Z. Yao, S. Yi, J. Shao, J. Yan, S. Wang, H. Li, and X. Wang. Orientation invariant feature embedding and spatial temporal regularization for vehicle re-identification. In *ICCV*, pages 379–387, 2017.
- [35] J.-R. Chang and Y.-S. Chen. Pyramid stereo matching network. In *CVPR*, pages 5410–5418, 2018.
- [36] V. Casser, S. Pirk, R. Mahjourian, and A. Angelova. Depth prediction without the sensors: Leveraging structure for unsupervised learning from monocular videos. In *AAAI*, volume 33, pages 8001–8008, 2019.
- [37] B. Bozorgtabar, M. S. Rad, D. Mahapatra, and J.-P. Thiran. Syndemo: Synergistic deep feature alignment for joint learning of depth and ego-motion. In *ICCV*, pages 4210–4219, 2019.
- [38] Y. Zou, Z. Luo, and J.-B. Huang. Df-net: Unsupervised joint learning of depth and flow using cross-task consistency. In *ECCV*, pages 36–53, 2018.
- [39] N. Mayer, E. Ilg, P. Hausser, P. Fischer, D. Cremers, A. Dosovitskiy, and T. Brox. A large dataset to train convolutional networks for disparity, optical flow, and scene flow estimation. In *CVPR*, pages 4040–4048, 2016.

- [40] C. Zheng, T.-J. Cham, and J. Cai. T2net: Synthetic-to-realistic translation for solving single-image depth estimation tasks. In *ECCV*, pages 767–783, 2018.
- [41] X. Fei, A. Wong, and S. Soatto. Geo-supervised visual depth prediction. *RA-L*, 4(2):1661–1668, 2019.
- [42] Y. Kuznetsov, J. Stuckler, and B. Leibe. Semi-supervised deep learning for monocular depth map prediction. In *CVPR*, pages 6647–6655, 2017.
- [43] C. Godard, O. Mac Aodha, and G. J. Brostow. Unsupervised monocular depth estimation with left-right consistency. In *CVPR*, pages 270–279, 2017.
- [44] F. Chollet. Xception: Deep learning with depthwise separable convolutions. In *CVPR*, pages 1251–1258, 2017.
- [45] A. G. Howard, M. Zhu, B. Chen, D. Kalenichenko, W. Wang, T. Weyand, M. Andreetto, and H. Adam. Mobilenets: Efficient convolutional neural networks for mobile vision applications. *arXiv preprint arXiv:1704.04861*, 2017.
- [46] D. G. Lowe. Distinctive image features from scale-invariant keypoints. *IJCV*, 60(2):91–110, 2004.
- [47] O. Russakovsky, J. Deng, H. Su, J. Krause, S. Satheesh, S. Ma, Z. Huang, A. Karpathy, A. Khosla, M. Bernstein, et al. Imagenet large scale visual recognition challenge. *IJCV*, 115(3):211–252, 2015.
- [48] J. H. Lee, M.-K. Han, D. W. Ko, and I. H. Suh. From big to small: Multi-scale local planar guidance for monocular depth estimation. *arXiv preprint arXiv:1907.10326*, 2019.
- [49] D. P. Kingma and J. Ba. Adam: A method for stochastic optimization. *arXiv preprint arXiv:1412.6980*, 2014.